Supplementary Information for

Hydrogen Adsorption in Azolium and Metalated N-Heterocyclic Carbene Containing MOFs

Patrick K. Capon,[a] Alexandre Burgun,[a] Campbell J. Coghlan,[a] Rachel S. Crees,[a] Christian J. Doonan*[a] and Christopher J. Sumby*[a]

a. *Centre of Advanced Nanomaterials and the School of Physical Sciences, The University of Adelaide, Adelaide, South Australia 5005, Australia.* CJD, e-mail: christian.doonan@adelaide.edu.au; CJS, e-mail: christopher.sumby@adelaide.edu.au.

Table of Contents

Crystallographic Data

Table S1. X-Ray experimental data for all MOFs synthesised using **H_3LBr**.

Compound	**1-Cu (Zn@Cu)**	**2 (Cu)**	**3 (Co)**	**4 (Mg)**	**5 (Mn)**
Empirical formula	$C_{72.25}H_{50.25}Br_{1.2}Cu_{1.2}N_{10.55}O_{26.15}Zn_4$	$C_{40.25}H_{35.15}Br_{0.1}Cu_{2.1}N_{6.65}O_{14.45}$	$C_{75.5}H_{69.5}N_{12.5}O_{28.5}Co_3$	$C_{74}H_{66}Mg_3N_{12}O_{28}$	$C_{72.5}H_{60.5}Mn_3N_{11.5}O_{26.5}$
Formula weight	1918.20	984.62	1784.72	1644.31	1681.64
Crystal system	monoclinic	monoclinic	monoclinic	triclinic	triclinic
Space group	C2/m	C2/m	C2/c	P-1	P-1
a (Å)	20.889(4)	20.7373(16)	23.128(5)	10.393(2)	11.014(2)
b (Å)	18.004(4)	17.9433(14)	14.043(3)	14.018(3)	13.053(3)
c (Å)	10.913(2)	10.9131(8)	23.412(5)	14.240(3)	14.145(3)
α (°)	90	90	90	117.59(3)	63.88(3)
β (°)	91.36(3)	91.48(7)	95.37(3)	93.18(3)	79.87(3)
γ (°)	90	90	90	98.27(3)	89.57(3)
Volume ($Å^3$)	4103.1(14)	4059.4(5)	7571(3)	1801.9(8)	1791.8(8)
Z	2	4	4	1	1
Density (calc.) g/m^3	1.553	1.611	1.566	1.515	1.558
Absorption coefficient (mm^{-1})	2.124	1.277	0.746	0.141	0.615
F(000)	1927	2013	3676.0	854.0	863.0
Crystal size (mm^3)	0.25 x 0.2 x 0.2	0.3 x 0.15 x 0.15	0.28 x 0.14 x 0.10	0.1 x 0.1 x 0.05	0.28 x 0.14 x 0.12
2θ range for collection (°)	2.986 to 60.17	5.352 to 58.392	3.396 to 55.84	3.258 to 55.838	3.268 to 55.828
Reflections collected	41452	18655	62700	30454	30395
Observed reflections [R(int)]	5725 [0.0853]	5081 [0.0536]	9027 [0.0245]	7830 [0.0361]	7854 [0.0706]
Goodness-of-fit on F_2	1.055	1.074	1.048	1.056	1.060
R_1 [I>2σ(I)]	0.0760	0.0583	0.0453	0.0532	0.0788
wR_2 (all data)	0.2127	0.1685	0.1199	0.1422	0.2330
Largest diff. peak and hole ($e.Å^{-3}$)	4.57, -4.04	2.58, -0.98	0.86, -0.81	0.35, -0.76	2.92, -0.79

FTIR Spectra for 1-5

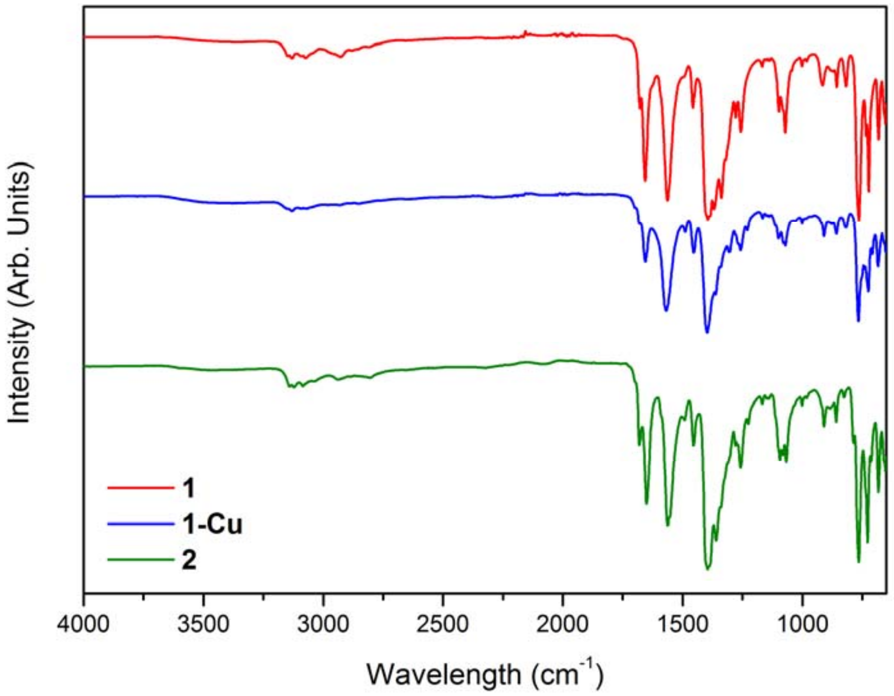

Fig. S1. FTIR spectra for **1**, **1-Cu**, and **2**, showing similar features due to the isomorphous nature of all three MOFs.

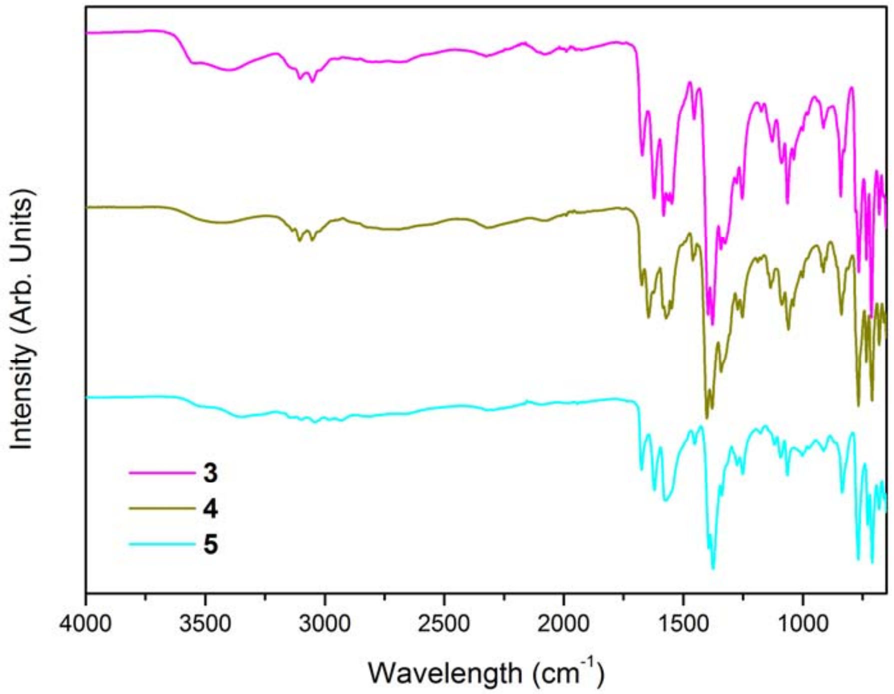

Fig. S2. FTIR spectra for **3**, **4**, and **5**, showing similar features due to the isostructural nature of all three MOFs.

Crystal Images of 1-Cu and 2

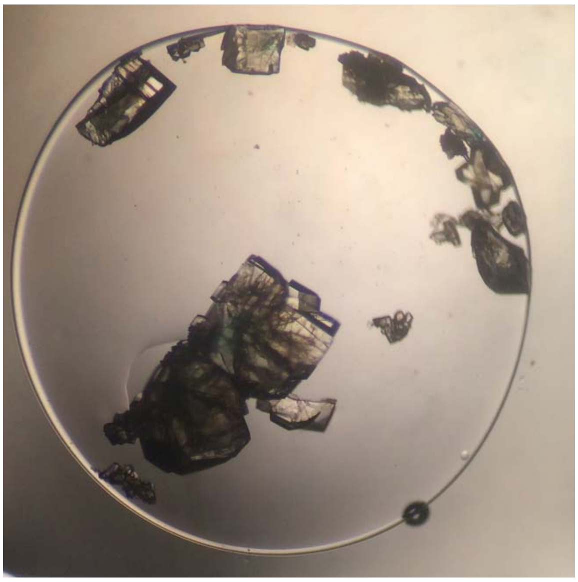

Fig. S3. Pure crystalline sample of **1-Cu** viewed down an optical microscope at 35x magnification.

Fig. S4. Pure crystalline sample of **2** viewed down an optical microscope at 35x magnification.

Powder X-Ray Diffraction Data for 3, 4, and 5

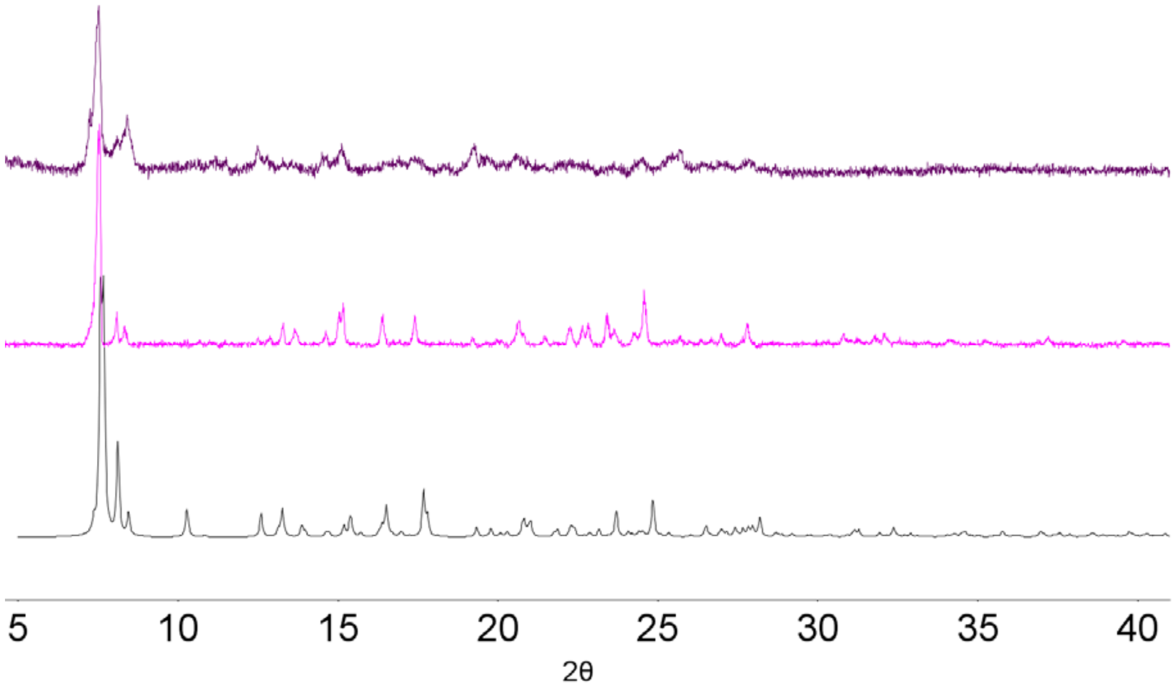

Fig. S5. PXRD patterns of **3**; theoretical (black), as synthesised (pink), and heated to 100°C (purple). A loss in crystallinity was observed after heating, indicating the framework is unstable toward solvent loss.

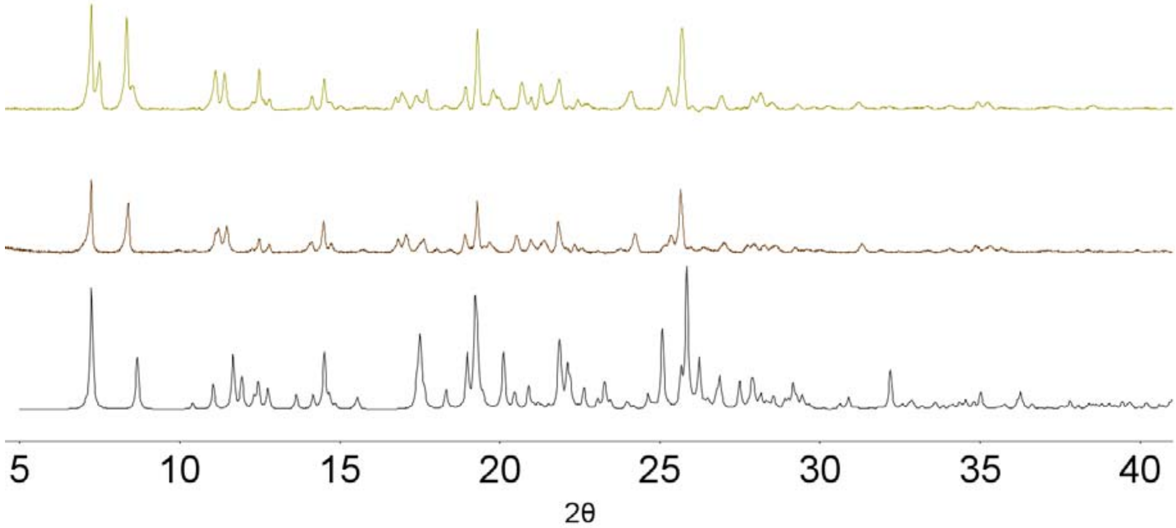

Fig. S6. PXRD patterns of **4**; theoretical (black), as synthesised (brown), and heated to 100°C (gold). No loss in crystallinity was observed for this samples after heating.

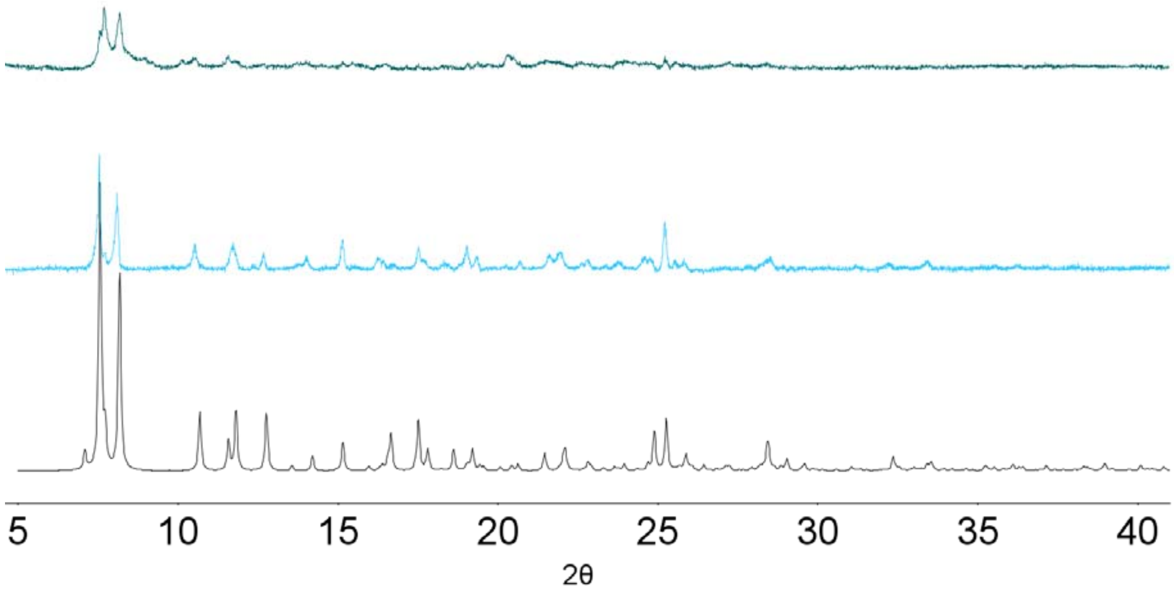

Fig. S7. PXRD patterns of **5**; theoretical (black), as synthesised (light blue), and heated to 100°C (dark aqua). A loss in crystallinity was observed after heating, indicating the framework is unstable toward solvent loss.

Crystal Images of 3-5

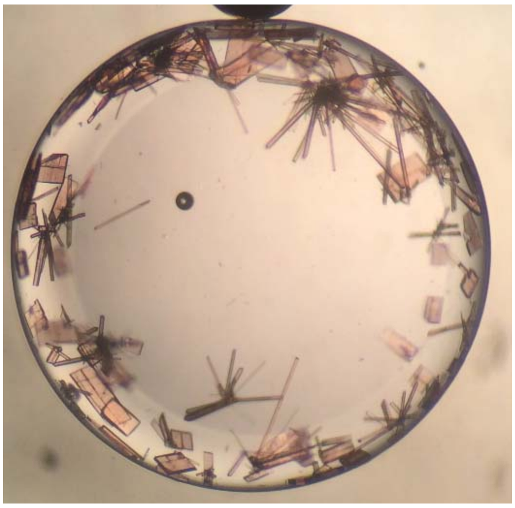

Fig. S8. Pure crystalline sample of **3** viewed down an optical microscope at 35x magnification.

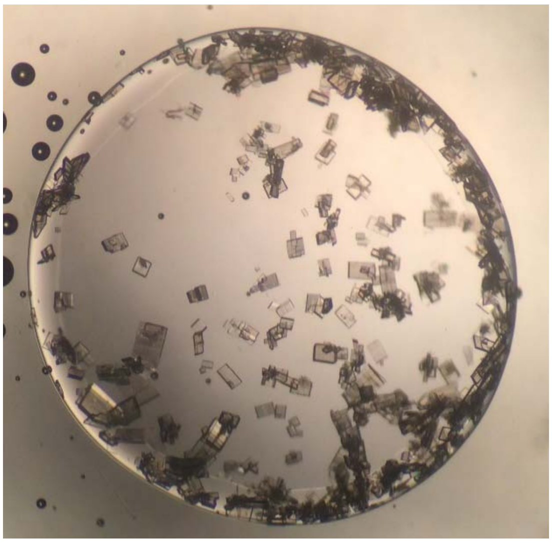

Fig. S9. Pure crystalline sample of **4** viewed down an optical microscope at 35x magnification.

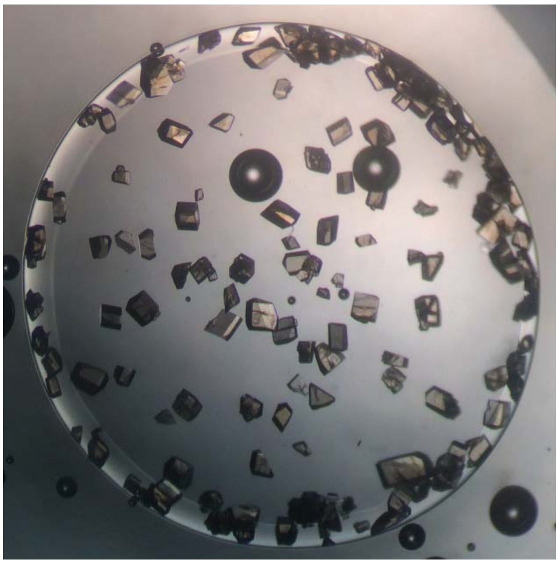

Fig. S10. Pure crystalline sample of **5** viewed down an optical microscope at 35x magnification.

Extent of Metalation in of 1-Cu

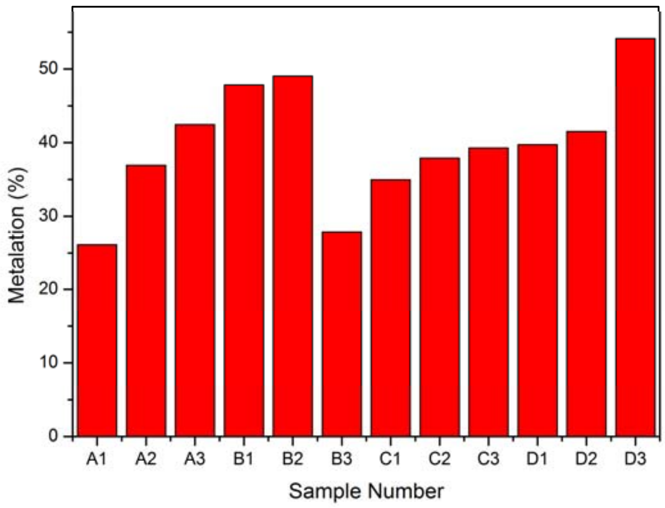

Fig. S11. Variation of Cu(I) metalation between samples of **1-Cu** was investigated by ICP-MS. Three individual crystals were studied from four separate vials to gives samples A1-3, B1-3 and so forth.

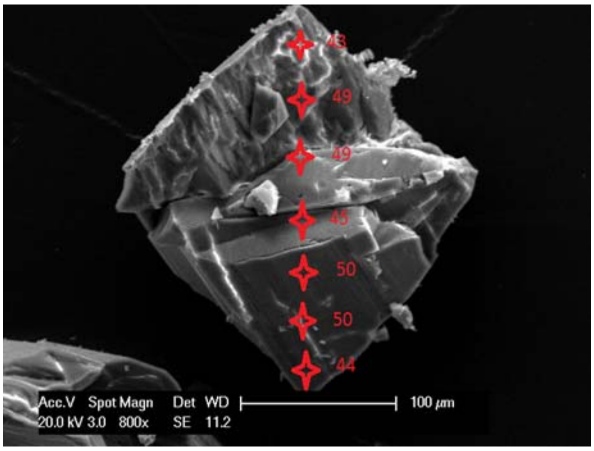

Fig. S12. EDX of the exposed inner face of a crystal of **1-Cu** with the metalation percentage of Cu(I) in red, and the approximate collection point shown by the red star symbol.

TGA of 1, 1-Cu, and 2

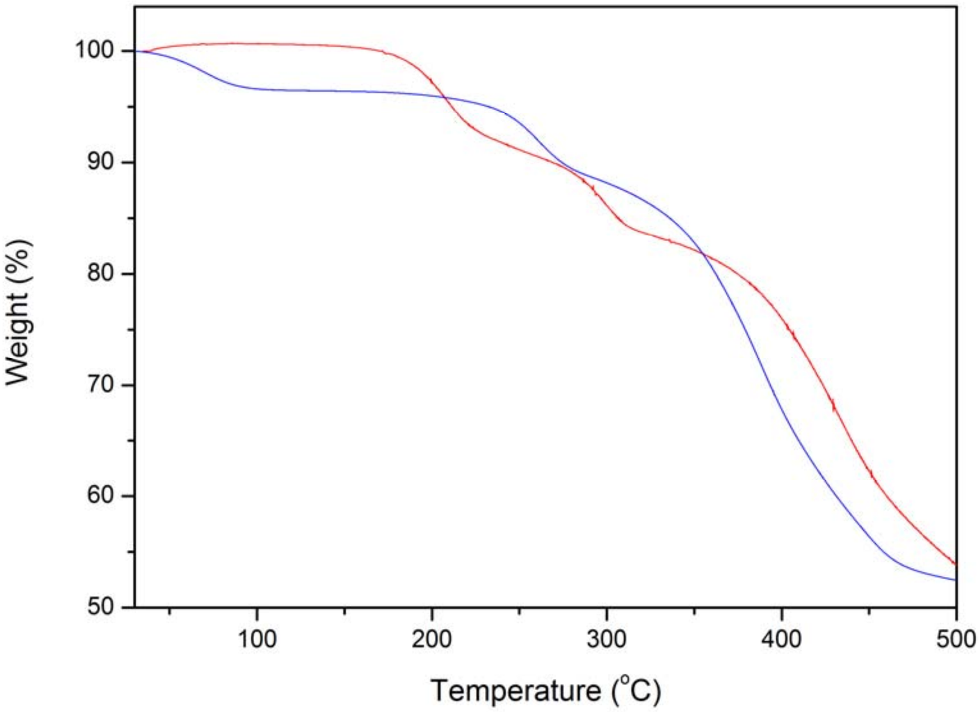

Fig. S13. TGA for **1-Cu** (red), and **1-Cu**^{act} (blue) showing DMF loss from the as synthesised framework between 160 and 220°C, and the hygroscopic nature of **1-Cu**^{act}.

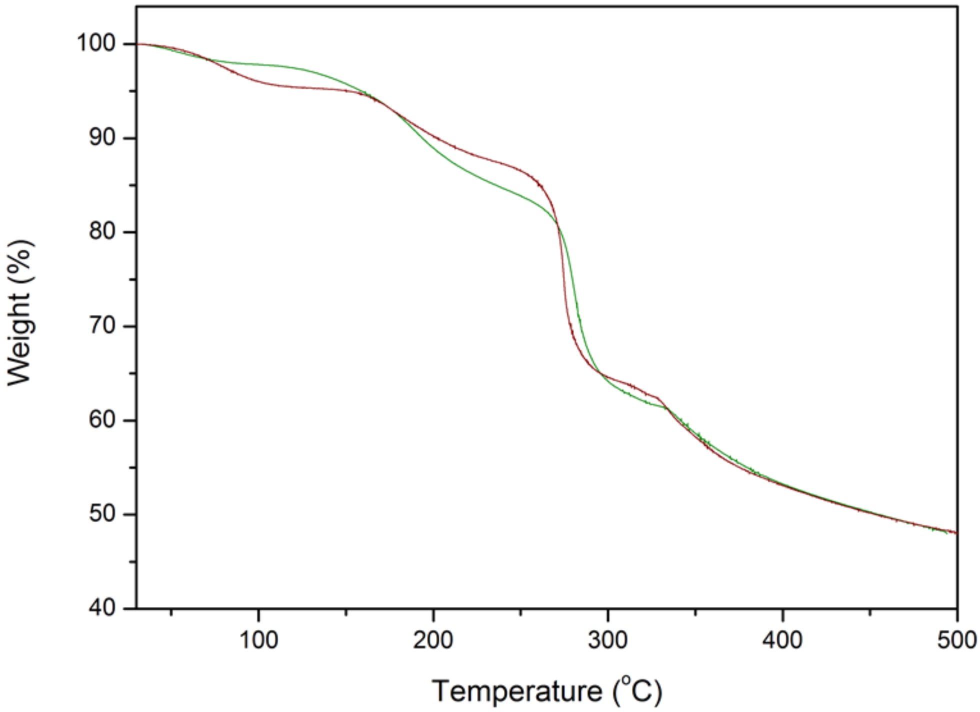

Fig. S14. TGA for **2** (green), and **2**^{act} (brown) showing DMF loss from the as synthesised framework between 160 and 220°C, and the hygroscopic nature of **2**^{act}.

Activated Powder X-Ray Diffraction for 1, 1-Cu, and 2

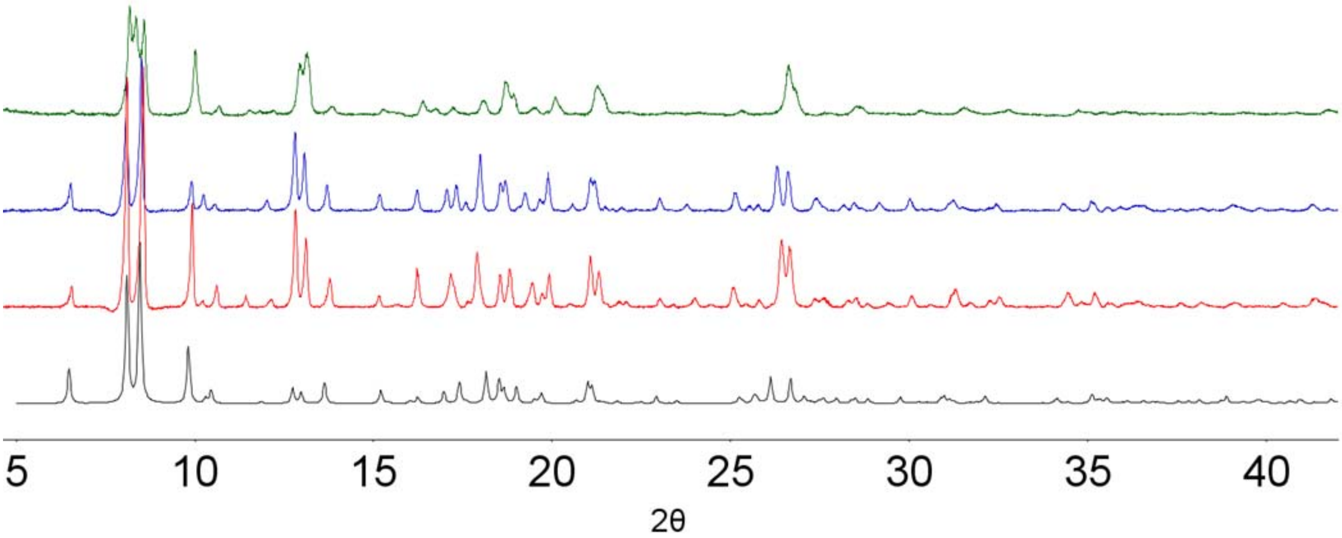

Fig. S15. PXRD patterns of **1** theoretical (black), $\mathbf{1}^{act}$ (red), $\mathbf{1\text{-}Cu}^{act}$ (blue), and $\mathbf{2}^{act}$ (green), showing retention of crystallinity for **1** and **1-Cu**, with a minor loss of crystallinity observed for **2**.

Pore Space Imaging of 1, 1-Cu and 2

For all figures below, the interior surface of the solvent accessible pore volume is shown in yellow and the exterior surface is grey. Pore spaces are shown slightly transparent for clarity.

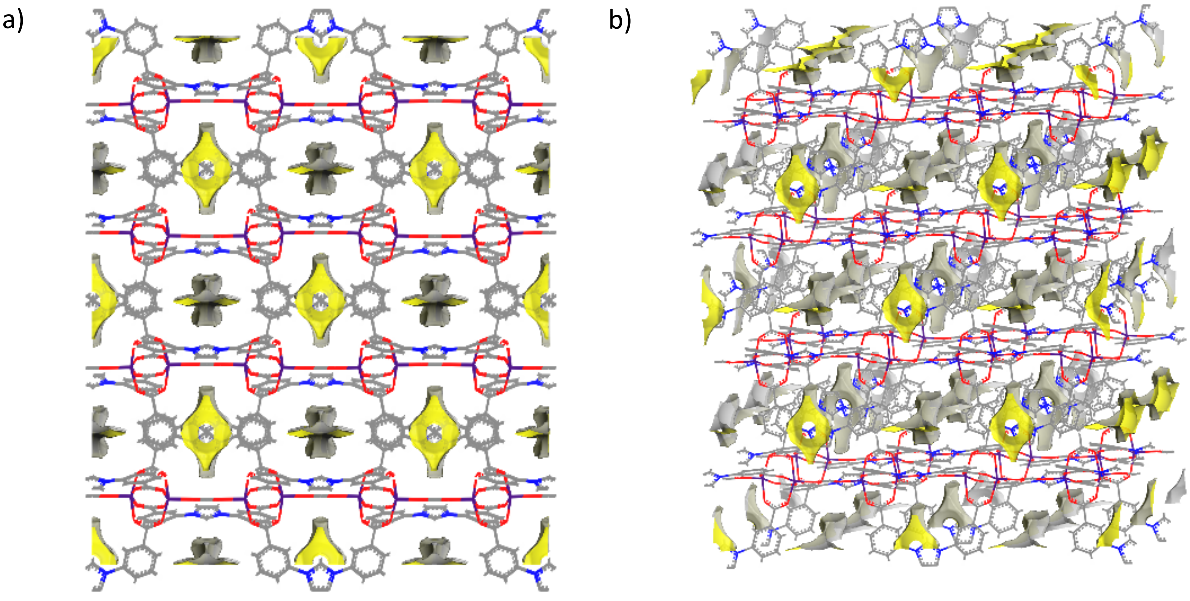

Fig. S16. Solvent accessible pore space in **1** viewed **a)** down the c axis and **b)** tilted off the c axis to show the extension of the pore channels through the framework. This figure also applies for framework **2** with appropriate substitution of Zn(II) for Cu(II).

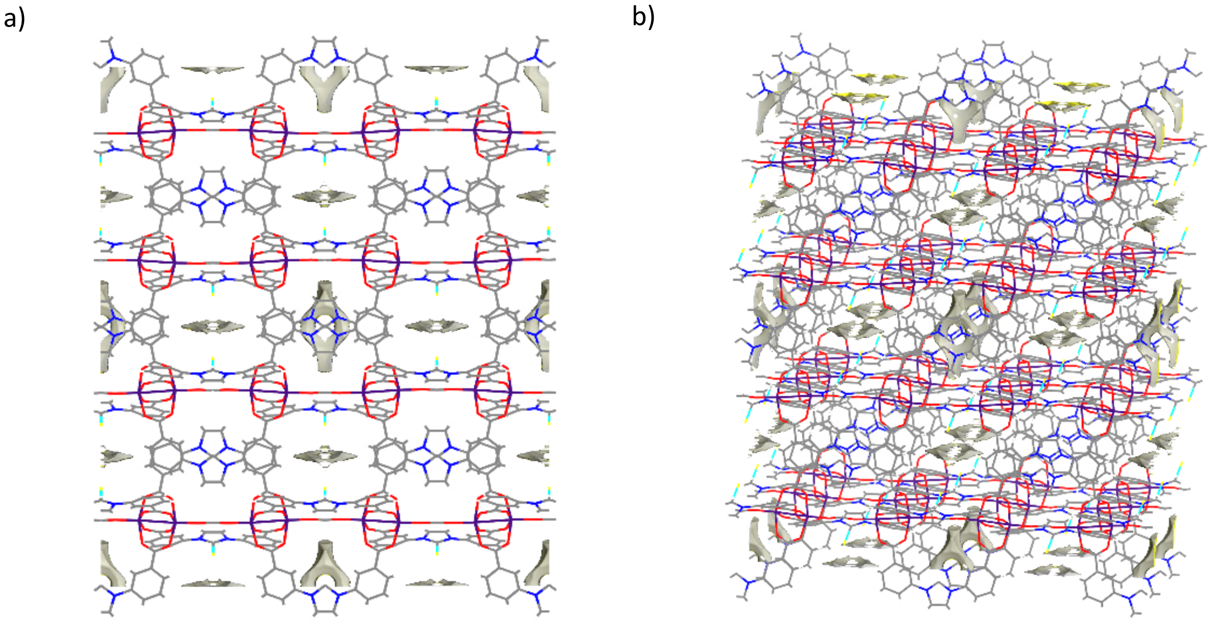

Fig. S17. Solvent accessible pore space in **1-CuA** viewed **a)** down the c axis and **b)** tilted off the c axis. The accessible pore volume has been greatly reduced compared to that of **1** due to the NHC-Cu-Br moiety protruding into the pore, reflecting the significantly lower BET surface area calculated (160 m^2g^{-1}).

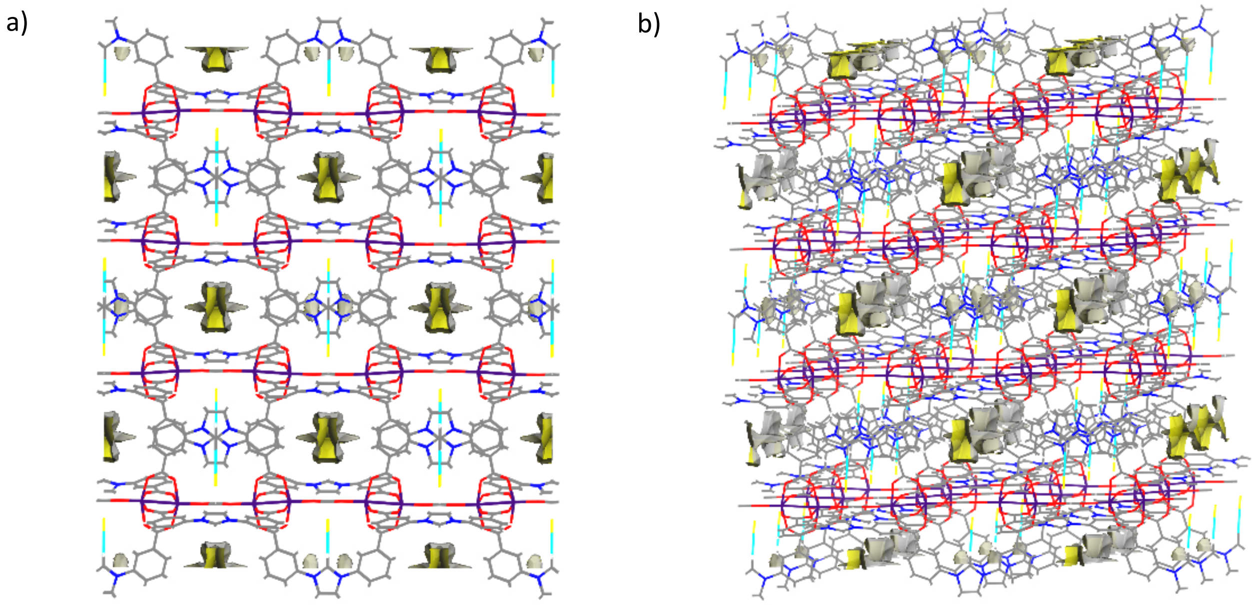

Fig. S18. Solvent accessible pore space in **1-CuB** viewed **a)** down the c axis and **b)** tilted off the c axis to show the extension of the pore channels through the framework. Note that there is minimal difference in accessible pore space when compared to **1,** as predicted by the theoretical BET surface area (340 m^2g^{-1}).

87 K H_2 Isotherms

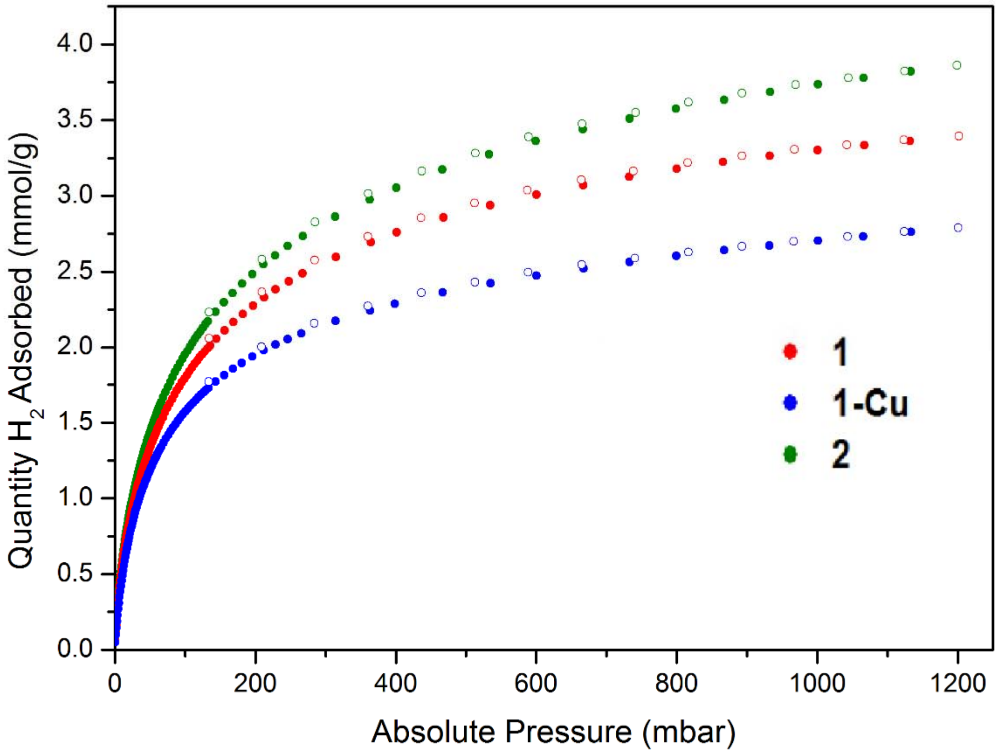

Fig. S19. H_2 adsorption isotherms for **1**, **1-Cu**, and **2** at 87 K. Filled circles indicate adsorption while empty circles indicate desorption.

Q_{st} Values from Van’t Hoff Plots

Table S2. Low coverage Q_{st} values obtained from proprietary software on the Micromeritics 3-Flex Analyser.

MOF	**Low coverage Q_{st} value (kJmol^{-1})**
1	-9.189
1-Cu	-8.999
2	-9.093

Pore Size Distribution of 1, 1-Cu, and 2

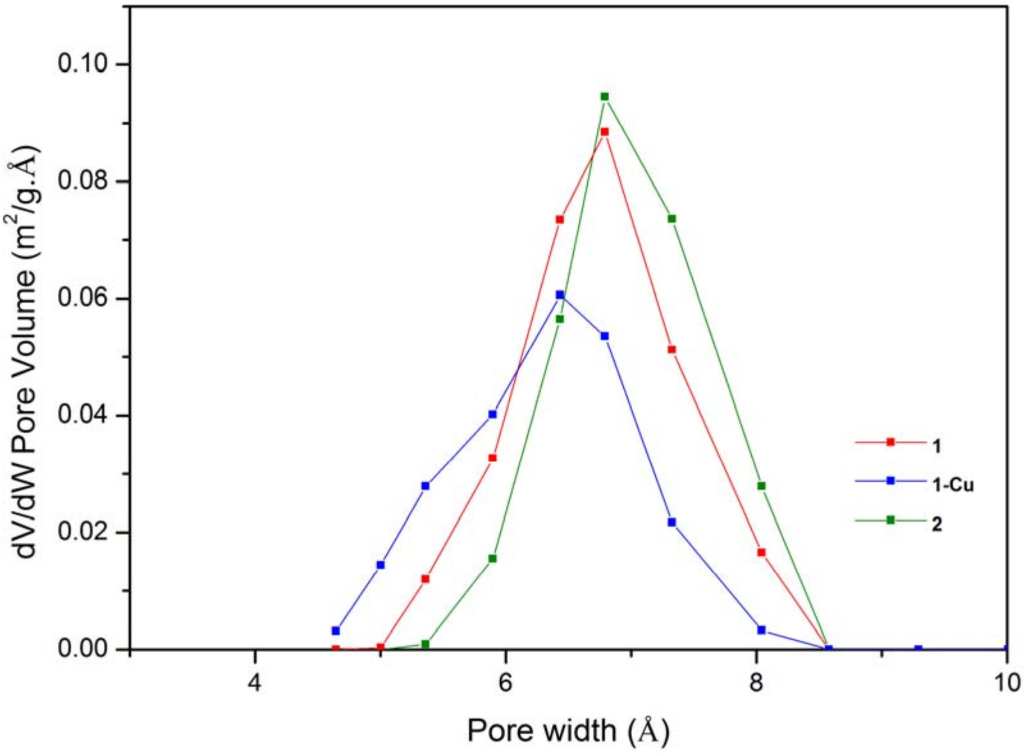

Fig. S20. Calculated pore size distributions for **1**, **1-Cu**, and **2**, indicating the slightly smaller pores in **1-Cu** resulting from partial metalation of the imidazolium present in **1** to form an NHC-CuBr moiety.